Journal of Physics and Chemistry of Solids 138 (2020) 109276

Contents lists available at ScienceDirect

Journal of Physics and Chemistry of Solids

journal homepage: http://www.elsevier.com/locate/jpcs

New gold chalcogenides in the Au–Te–Se–S system

Galina Palyanova [a,b], Yuri Mikhlin [c,*], Veronika Zinina [a,b], Konstantin Kokh [a,b], Yurii Seryotkin [a,b], Tatyana Zhuravkova [a,b]

[a] Sobolev Institute of Geology and Mineralogy, Siberian Branch of the RAS, Koptyuga Ave., 3, Novosibirsk, 630090, Russia
[b] Novosibirsk State University, Pirogova Str., 2, Novosibirsk, 630090, Russia
[c] Institute of Chemistry and Chemical Technology, Krasnoyarsk Science Center, Siberian Branch of the RAS, Akademgorodok, 50/24, Krasnoyarsk, 660036, Russia

ARTICLE INFO

Keywords:
Gold chalcogenides
Pyrosynthesis
SEM
X-ray diffraction
Raman spectroscopy
X-ray photoelectron spectroscopy

ABSTRACT

The pyrosynthesis of gold chalcogenides AuX ($AuTe_{0.7}Se_{0.2}S_{0.1}$), AuX_2 ($AuTe_{1.8}Se_{0.2}$–$AuTe_{1.8}Se_{0.1}S_{0.1}$) and Au_3X_{10} ($Au_3Te_6Se_3S$–$Au_3Te_6Se_{2.5}S_{1.5}$) was performed from a mixture of elemental substances taken in the atomic ratios X/Au (X = Σ(Te + Se + S)) of $AuTe_{0.666}Se_{0.167}S_{0.167}$ (X/Au = 1), $AuTeSe_{0.5}S_{0.5}$ (X/Au = 2), $AuTe_2Se_{1.125}S_{0.375}$, $AuTe_2Se_{0.75}S_{0.75}$ (X/Au = 3.5) and $AuTe_{2.5}SeS_{0.5}$ (X/Au = 4). Optical and scanning electron microscopy, electron microprobe analysis, X-ray powder diffraction, X-ray photoelectron spectroscopy and Raman spectroscopy were applied to characterize the samples. It was established that Au chalcogenides of composition AuX_2 were analogous to mineral calaverite ($AuTe_2$), Au_3X_{10} phases were close to S-bearing mineral maletoyvayamite and the AuX substance seemed to be a synthetic analog of a phase $Au_{0.99–1.00}Te_{0.70–0.71}Se_{0.25–0.27}S_{0.03–0.06}$ found in the Gaching area of the Maletoivayam ore field (Central Kamchatka volcanic belt). The results on complex Au chalcogenides in the quaternary Au–Te–Se–S system are of interest for chemistry, mineralogy and geochemistry of Au, and potential applications in materials science.

1. Introduction

Gold (Au) is one of the least reactive chemical elements that forms a number of compounds with chalcogens [1–21]. Simple Au chalcogenides have been synthesized in binary (Au–tellurium (Te), Au–selenium (Se) and Au–sulfur (S)) [1–3,5,14,16–19] and ternary Au–S–Te systems [1,6,7]. The Au sulfides Au_2S and Au_2S_3 are unstable and decompose to the elements [2]. There are stable α- and β-$AuTe_2$ phases ([5] and references therein) and Au_2Te_3 [14], and the existence of $AuTe_3$ and AuTe compounds were predicted by Rong et al. [12] and Streltsov et al. [13] in the Au–Te system, but these last phases have not been found yet. Two different crystallographic modifications, α- and β-AuSe, are known for the Au–Se system [1,16,20]. In the ternary Au–Se–Te system, the Au_2SeTe phase [1] and solid solution $Au_2Se_3Te_4$–$Au_4Se_5Te_8$ [6] have been found. Tuhý et al. [7] synthesized two ternary compounds, Au_2TeSe and $Au_3Te_6Se_4$, related to solid solutions in the range of $Au_2Te_{0.94}Se_{1.11}$–$Au_2Te_{1.58}Se_{0.49}$ and $Au_3Te_{6.06}Se_{4.18}$–$Au_3Te_{6.58}Se_{3.87}$, respectively, in which Se replaced Te. Some special properties are possible in such materials; for example, Luo et al. [10] reported that metastable Au_3Te_5 is a superconductor at very low temperatures, while $AuTe_2$ having an incommensurate crystal structure becomes superconducting at elevated pressure or upon doping with platinum metal [13]. Nevertheless, the properties of Au chalcogenides are insufficiently understood.

In nature, Au mainly occurs in elemental form, but several Au chalcogenide minerals are also known in the Au–S–Se–Te system, including calaverite ($AuTe_2$) [8–14,22–25] and montbrayite (Au_2Te_3) [22,24,26–31]. These phases are actually non-stoichiometric, with additional elements, particularly silver, stabilizing the structures [3,4,24,26–31]. Bindi et al. [21] recently demonstrated the chemical formula of montbrayite to be $(Au,Ag,Sb,Pb,Bi)_{23}(Te,Sb,Pb,Bi)_{38}$ rather than Au_2Te_3 [3,4]. Generally, Au chalcogenides are minor minerals in ores of Au [32–34], but recently an uncommon noble metal mineralization was found in the Gaching ore occurrence (Maletoivayamore field, Central Kamchatka volcanic belt) [35–37], which contains calaverite with minor amounts of Se and S, along with S–Se–tellurides $Au_2Te_4Se_3$, $Au_2Te_4S_3$ and their solid solutions including $Au_2Te_4(S,Se)_3$, $Au_3(Te,Se,S)_{10}$, AuSe and Au(Te,Se,S). The $Au_3Te_6Se_4$ phase was recently approved as a new mineral maletoyvayamite [38].

To the best of our knowledge, data on the synthesis and compositions of quaternary Au–S–Se–Te compounds are unavailable in literature, and chemical Au–chalcogen bonding is still poorly understood. Therefore,

* Corresponding author.
E-mail address: yumikh@icct.ru (Y. Mikhlin).

https://doi.org/10.1016/j.jpcs.2019.109276
Received 3 July 2019; Received in revised form 20 November 2019; Accepted 21 November 2019
Available online 22 November 2019
0022-3697/

the aim of this work was to obtain stable chalcogenides in the Au–S–Se–Te system and to study some of their characteristics.

2. Experiments and analytical methods

Gold (99.99%), S, Se and Te (99.9%) were employed as starting materials for synthesis experiments. The weighing accuracy was 0.05 mg (Mettler Instrument Ag CH-8606 Greifensee-Zurich). The Au chalcogenides were synthesized by heating the mixtures of elementary substances with the atomic ratios of X = Σ(Te + Se + S) to Au from 1 to 4: Au 1, Te 0.667, Se 0.167, S 0.167 (X/Au = 1); Au 1, Te 1, Se 0.5, S 0.5 (X/Au = 2); Au 1, Te 2, Se 1.125, S 0.375; Au 1, Te 2, Se 0.75, S 0.75 (X/Au = 3.5); Au 1, Te 2.5, Se 1, S 0.5 (X/Au = 4), with Te/(S + Se) = 2, 1.67, 1.33 and 1 (Tables 1 and 2). The quartz vessels with the initial mixtures were evacuated and sealed [37].

In the experiments with initial compositions AuX, $AuX_{3.5}$ and AuX_4 (Nos. 1 and 4, Table 1, and No. 5, Table 2), quartz ampoules were heated to 600°C at 100 °C/h then to 700 °C at 10 °C/h, kept at this temperature for 5 days, then cooled to 400 °C at 50°/h and annealed for 14 days. In experiments No. 2 and 3 (Table 1) with initial compositions AuX_2 and $AuX_{3.5}$, respectively, quartz ampoules were heated to 400°C at 100 °C/h, then to 550°C at 20 °C/h, up to 600 °C at 20 °C/h, kept at this temperature for 3 days, then cooled to 400 °C at 50 °C/h and annealed for 14 days. In the synthesis with initial composition $AuX_{3.5}$ (No. 6, Table 2), the ampoule was annealed at 500 °C. After annealing, the ampoules were cooled to room temperature in the off mode of the furnace.

Optical microscopy, scanning electron microscopy (SEM), electron microprobe analysis (EPMA), X-ray powder diffraction (XRD), X-ray photoelectron spectroscopy (XPS) and Raman spectroscopy (RS) were applied to study the synthesized samples. A polished section was prepared from 1/3 of each sample. Chemical analyses of synthesized phases were carried out using a MIRA LMU electron scanning microscope (TESCAN) with an INCA Energy 450+ X-Max energy-dispersion spectrometer (Oxford Instruments). Operation conditions were as follows: accelerating voltage was 20 kV, probe current was 1 nA and spectrum recording time was 15–20 s. In all measurements the electron beam was slightly defocused to reduce the effect of sample microrelief and the destructive influence of the beam on unstable Au chalcogenides. Pure Au, $CuFeS_2$, PbSe and Ag_2Te were used as standards for Au, S, Se and Te, respectively. The analysis accuracy was 1–1.5 relative %.

The XRD experiments were performed using a Stoe STADI MP X-ray powder diffractometer (Cu $K_{\alpha 1}$ radiation, Ge (111) monochromator, 40 kV, 40 mA) equipped with a linear Mythen 1 K detector. Powder diffraction patterns were collected over the 2θ angular range of 5–50° with a step of 0.015°. Phase analysis was carried out using the PDF-4 database [39].

Raman spectra of Au chalcogenides were acquired on a Ramanor U–1000 spectrometer, with detector JobinYvon LabRAM HR800 and a laser MillenniaPro (Spectra–Physics) with nominal wavelength λ = 532 nm. An upright microscope Olympus BX-51 WI with a 100 × magnifying objective was used to direct the laser beam onto the sample and to collect the Raman signal under the following parameters: spectral resolution of 2.09 cm^{-1}, exposure time of 10 s, five repetitions and filtration D1. The spectra were calibrated against the emission lines of a standard neon lamp, and the peak positions were accurate to within ±0.2 cm^{-1}.

The X-ray photoelectron spectra were measured from materials crushed immediately before the experiment and attached to carbon tape with a SPECS spectrometer equipped with a PHOIBOS 150 MCD-9 analyzer at electron take-off angle 90° with monochromatic Al Kα radiation (1486.6 eV). The analyzer pass energy was 10 eV for high-resolution spectra. After subtraction of Shirley-type background, the Au $4f_{7/2,5/2}$, Se $3d_{5/2,3/2}$ and S $2p_{3/2,1/2}$ doublets were fitted employing Gaussian–Lorentzian peak shape, spin–orbit splitting of 3.67, 0.88 and 1.19 eV and branching ratios of 0.75, 0.667 and 0.5, respectively, using CasaXPS software.

Table 1
Initial composition (atomic ratios) and results of experiments at annealing temperature of 400°C, determined using electron probe microanalysis.

No	Initial mixtures	Composition and yield (vol.) of main products	Abbreviation of phases
1	Au 1, Te 0.667, Se 0.167, S 0.167 (X/Au = 1, Te/(S + Se) = 2, Se/S = 1)	$Au_3Te_6Se_{2.5}S_{1.5}$ (30%) $AuTe_{1.8}Se_{0.1}S_{0.1}$ (20%) $AuTe_{0.7}Se_{0.2}S_{0.1}$ (10%) Au (40%)	Au_3X_{10} AuX_2 AuX Au
2	Au 1, Te 1, Se 0.5, S 0.5 (X/Au = 2, Te/(S + Se) = 1, Se/S = 1)	$Au_3Te_6Se_{2.5}S_{1.5}$ (25%) $AuTe_{1.8}Se_{0.2}$ (40%) $AuTe_{0.7}Se_{0.2}S_{0.1}$ (15%) Au (10%) $Te_{0.16}S_{0.5}Se_{0.34}$ (10%)	Au_3X_{10} AuX_2 AuX Au X
3	Au 1, Te 2, Se 1.125, S 0.375 (X/Au = 3.5, Te/(S + Se) = 1.333, Se/S = 3)	$Au_3Te_6Se_3S_1$ (35%) $AuTe_{1.8}Se_{0.1}S_{0.1}$ (20%) $AuTe_{0.7}Se_{0.2}S_{0.1}$ (15%) Au (5%) $Te_{0.29}S_{0.25}Se_{0.45}$ (25%)	Au_3X_{10} AuX_2 AuX Au X
4	Au 1, Te 2.5, Se 1, S 0.5 (X/Au = 4, Te/(S + Se) = 1.667, Se/S = 2)	$Au_3Te_6Se_{2.5}S_{1.5}$ (20%) $AuTe_{1.8}Se_{0.1}S_{0.1}$ (30%) $AuTe_{0.7}Se_{0.2}S_{0.1}$ (10%) Au (5%) $Te_{0.37}S_{0.32}Se_{0.31}$ (35%)	Au_3X_{10} AuX_2 AuX Au X

Table 2
Results of experiments with initial composition Au 1, Te 2, Se 0.75 and S 0.75 at different annealing temperatures, determined using electron probe microanalysis.

No	Atomic ratios in reaction mixtures, annealing temperatures	Composition and yield (vol.) of main products	Abbreviation of phases
5	X/Au = 3.5, Te/(S + Se) = 1.333, Se/S = 1400°C	$Au_3Te_6Se_{2.5}S_{1.5}$ (50%) $AuTe_{1.8}S_{0.1}Se_{0.1}$ (10%) $Te_{0.61}S_{0.09}Se_{0.30}$ (40%)	Au_3X_{10} AuX_2 X
6	X/Au = 3.5, Te/(S + Se) = 1.333, Se/S = 1500°C	$Au_3Te_6Se_{2.7}S_{1.3}$ (60%) $AuTe_{1.85}Se_{0.15}$ (35%) Au (5%)	Au_3X_{10} AuX_2 Au

3. Results and discussion

3.1. Phase composition

Table 1 shows the EPMA results of experiments with initial ratios of X/Au of 1–4, the ratio of Te/(S + Se) varying within 1–2 and annealing temperature of 400°C [37]. Table 2 compares the EPMA results of syntheses with the same initial composition X/Au 3.5 (Nos 5 and 6) and annealing temperatures of 400 and 500°C.

In the experiment with the lowest amounts of chalcogens and, hence, with the lowest ratio Σ(Te + Se + S)/Au = 1 (No. 1), four phases were found in the crystallization products, including metallic Au and three chalcogenides: AuX ($AuTe_{0.7}S_{0.1}Se_{0.2}$), AuX_2 ($AuTe_{1.8}Se_{0.1}S_{0.1}$) and Au_3X_{10} ($Au_3Te_6Se_3S$). It is worth noting that the synthesized gray ingot looked homogeneous [37]. Chalcogens (Te, Se and S) virtually completely reacted with Au, forming three successive Au chalcogenides. The Au contacts with the AuX phase were surrounded by AuX_2, which intergrew with the Au_3X_{10} phase (Fig. 1a and b). The phase, which was similar in composition to $AuTe_2$, contained minor amounts of S (to 0.28 wt%) and Se (to 2.3 wt%).

In the ingots from experiments with initial ratios X/Au = 2, 3.5 and 4 (Nos 2–4, Table 1), we revealed the same three Au chalcogenides as in the experiment with X/Au = 1 (No. 1) – AuX_2–$AuTe_{1.8}Se_{0.1}S_{0.1}$ (Nos 3 and 4) and $AuTe_{1.8}Se_{0.2}$ (No. 2), Au_3X_{10}–$Au_3Te_6Se_3S$ (Nos 3 and 4) and $Au_3Te_6Se_{2.5}S_{1.5}$ (No. 2) and AuX–$AuTe_{0.7}S_{0.1}Se_{0.2}$ (Nos 2–4) – along with metallic Au and some elemental chalcogen phases containing Te, Se and S (Nos 2–4). Compared to the experiment with initial composition X/Au = 1 (No 1), the amount of Au was considerably lower, and the

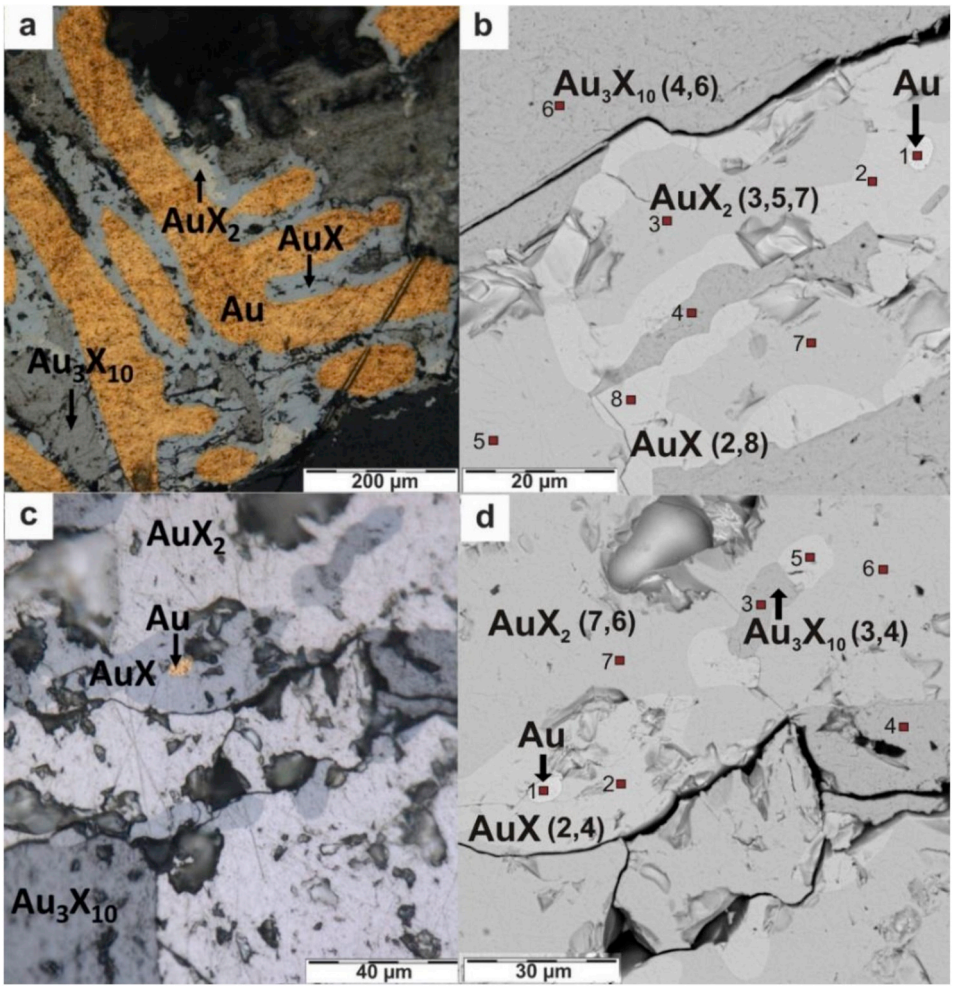

Fig. 1. Optical (a, c) and SEM (b, d) microphotographs of phases formed in the experiments with initial composition Au 1, Te 0.666, Se 0.167 and S 0.167 (X/Au = 1) (a, b) and Au 1, Te 2.5, Se 1 and S 0.5 (X/Au = 4) (c, d). Annealing temperature was 400°C (Nos 1 and 4, Table 1). The spots in which EPMA was performed are marked in (b, d).

quantity of the phase composed of a mixture of chalcogens increased, especially for X/Au = 4 (Fig. 1a, c, d; Table 1). Chalcogens were located in the intergranular space of Au chalcogenides, in the peripheral parts of the ingot and as microhemispheres on the ampoule walls. The following sequence of phases was observed around Au: Au → AuX → AuX_2 → Au_3X_{10} → X (Te, Se, S).

In experiments with the same initial ratios X/Au = 3.5 and S/Se = 1 (Table 2) but different annealing temperatures of 400°C (No. 5) and 500°C (No. 6), the phase Au_3X_{10} ($Au_3Te_6Se_3S$) was predominant while phase AuX was absent in the products, in contrast to syntheses 1–4. The ingot annealed at 400°C contained two Au chalcogenides ($Au_3Te_6Se_3S$ and $AuTe_{1.8}S_{0.1}Se_{0.1}$) and chalcogen phase ($Te_{0.6}Se_{0.3}S_{0.1}$) that formed skeletal structures (Fig. 2a and b). After annealing at 500°C, two chalcogenides $Au_3Te_6Se_3S$ and $AuTe_{1.8}S_{0.1}Se_{0.1}$ were also present, but the third phase was elemental Au (Fig. 2c and d).

3.2. XRD

The XRD patterns indicated that synthesized Au chalcogenide AuX_2 ($AuTe_{1.8}Se_{0.1}S_{0.1}$) corresponded to calaverite (α-$AuTe_2$) [18] (PDF card 01-074-7043) (Fig. 3). According to EPMA, the S and Se contents were 0.7 and 2.9 wt%, respectively, suggesting that they isomorphously replaced Te. All product samples contained phases with the crystalline structure of maletoyvayamite Au3Te6Se4 [38] (Fig. 3).

Peaks of metallic Au [39] (PDF card 03-065-8601) were observed in the diffractograms of the sample from experiment 6 (Table 1, Fig. 3). The elemental chalcogen phases formed in experiments 3–5 (Tables 1 and 2) exhibited reflections similar to Te [39] (PDF card 04-003-2449) or $Te_{0.5}Se_{0.5}$ (PDF card 01-003-7043) (Fig. 3). The diffractograms also contained unidentified peaks, including two or three peaks near 2θ of 30°, whose intensities varied for different samples thus implying the occurrence of two or more phases. Particularly, the intense reflections at 30.14° and 30.62° were observed for samples 3 and 4, whereas the first peak was much smaller and the last one was absent in the diffraction patterns of samples 5 and 6. Comparing the phases found using EPMA (Tables 1 and 2) suggests that these peaks arose from a new AuTe-based phase $AuTe_{0.7}Se_{0.2}S_{0.1}$, which is not present in databases. This compound was essentially absent from samples 5 and 6, probably because of a lower concentration of Se stabilizing the structure of AuX; it is noteworthy that AuSe phases were not found. We also propose that another unidentified phase was a compound of approximate composition of $Au_3Te_6Se_{2.5}S_{1.5}$ (Table 2) that was enriched in S compared with maletoyvayamite, and of a different crystal structure.

3.3. Raman spectroscopy

Raman spectra of synthetic Au chalcogenides AuX and Au_3X_{10} are shown in Fig. 4 in comparison with spectra of minerals from the Gaching ore occurrence [7,37]. Synthetic phase AuX ($AuTe_{0.7}Se_{0.2}S_{0.1}$) showed three bands at 130, 170 and 208 cm^{-1}, which were identical to those for new mineral phases of composition $Au_{0.99–1.00}Te_{0.70–0.71}Se_{0.25–0.27}S_{0.03–0.06}$ from the Gaching ore [7,37]. For AuX_2, both synthetic products

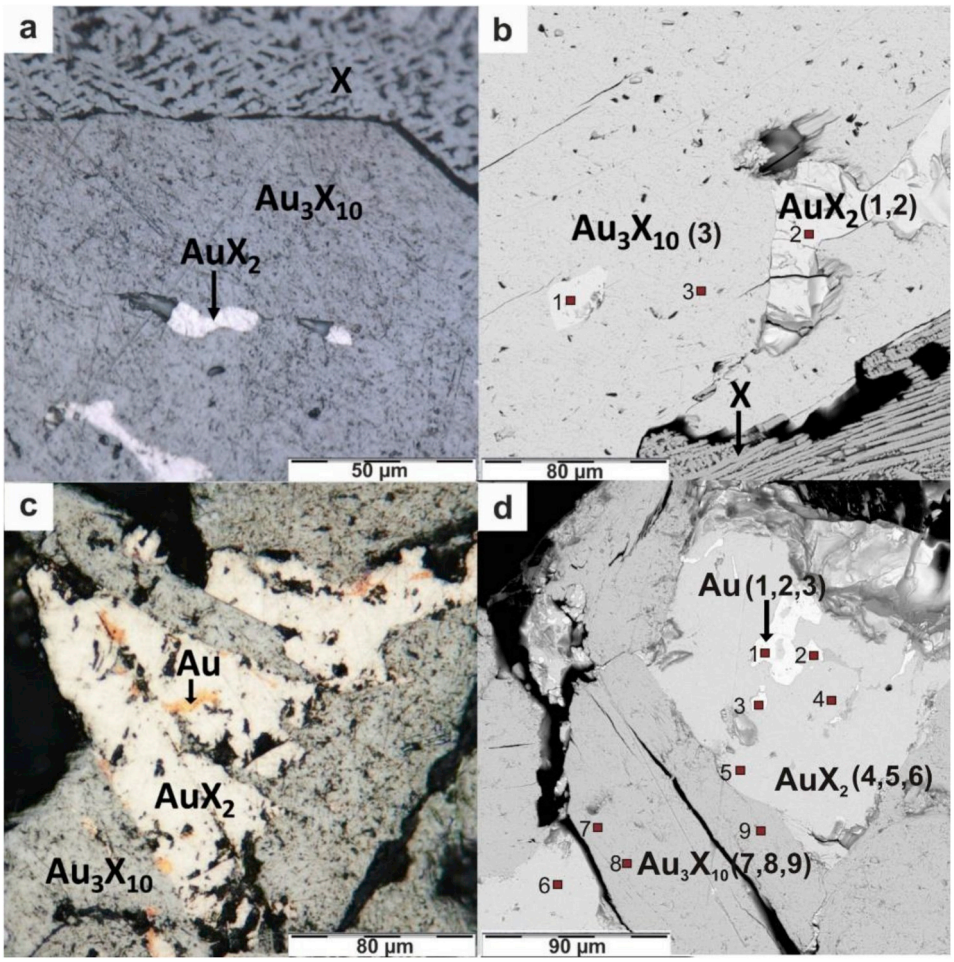

Fig. 2. Optical (a) and SEM (b) microphotographs of the products formed in the experiments with initial composition Au 1, Te 2, Se 0.75 and S 0.75 (X/Au = 3.5). Annealing temperatures were 400°C (a, b) and 500°C (c, d) (Nos 5 and 6, Table 2). The spots of EPMA are marked in (b, d).

$AuTe_{1.8}Se_{0.1}S_{0.1}$ and $AuTe_{1.8}Se_{0.2}$, and Gaching calaverite of composition $Au_{2.91–3.08}Te_{5.85–6.06}Se_{1.57–3.66}S_{2.63–0.44}$ [7,37] had a wide absorption band located at ~100 cm^{-1}.

Raman spectra of phases Au_3X_{10} ($Au_3Te_6Se_{2.5}S_{1.5}$ and $Au_3Te_6Se_3S$) showed bands at 101, 137 and 178 cm^{-1} that almost coincided with the peaks from natural maletoyvayamite [38] and its synthetic analog $Au_3Se_4Te_6$ [7]. Some differences, particularly the maxima at 277 and 322 cm^{-1} in the region characteristic of Te–Te and Se–Se stretching, seemed due to the presence of S and varying concentrations of chalcogens. Detailed interpretation of these and other spectral features requires further research. The similarity of the Raman spectra upon changing the concentrations of Se and S suggests similar structures and possible isomorphism in the range of $Au_3Te_6Se_4$–$Au_3Te_6Se_{2.5}S_{1.5}$.

3.4. XPS spectroscopy

The X-ray photoelectron spectra, which characterize the near-surface layers of about 2-nm thick, showed concentrations of Au and chalcogens close to the initial compositions of the reaction mixtures. The spectra of sample 1 (Table 1) differed from others because of a higher Au content (Fig. 5). The main peak Au $4f_{7/2}$ had the binding energy (BE) of 84.2 eV, which was only slightly higher than that of the bulk metal (84.0 eV); this can be attributed to surface Au^0–chalcogen bonding and/or the final-state effect typical for Au clusters formed via surface decomposition of binary Au chalcogenides [9,19–21]. This also agrees with the high content of elemental Au found with other techniques; the Au^0 seemed to contribute to the highest occupied states of the valence band. A component near 85 eV appeared to be due to Au^+ in Au chalcogenide phases, and a weaker line at 86.5 eV is attributable to Au^{3+} of surface Au oxide species in all the samples. As the content of chalcogens (X/Au ratio) increased, the low-energy Au 4f component shifted to 84.4–84.6 eV, and its relative intensity decreased, although retaining about 20–30% of total, whereas the line at the BEs of 85.2 eV increased; both of them seemed due to Au^+ in Au chalcogenide phases [6,9,19–24].

The main peak Te $3d_{5/2}$ had a BE of 573.15 eV for sample 1, and shifted to 573.6 eV for other samples (Table 1); these BEs may be assigned to Te^{2-} and Te^0, respectively. In addition, some spectra showed minor lines at about 575 and 576.5 eV from oxidized surface Te(IV) and Te(VI) species. The dominant S 2p component at 161.4 eV for all materials is characteristic of sulfide anion (S^{2-}). It is worth noting that the S 2p and Se 3p spectra overlapped each other, and their fitting was not quite unambiguous. Significant changes of the chemical state of Se were observed in the Se 3d spectra with varying ratios of the components at 53.8 and 55.2 eV, which are typical for Se^{2-} and Se^0 species, respectively. For sample 1, the spectrum was better fitted with the components at 53.6 and 54.6 eV.

For samples 5 and 6 (Table 2) with the initial composition of elements X/Au = 3.5 (Fig. 6), the Se $3d_{5/2}$ peak at 53.9 eV was much stronger than that at ~55 eV, while the Au 4f, Te 3d and S 2p spectra were basically similar to those for sample 4 (Table 1).

The exact origin of the XPS features is difficult to understand because of the multiphase composition of the samples. Nevertheless, since Au_3X_{10} compounds usually prevailed, we suggest that Au in these phases had the BE of 85.2 eV, and the lines at 84.4–84.8 eV belonged, at least in

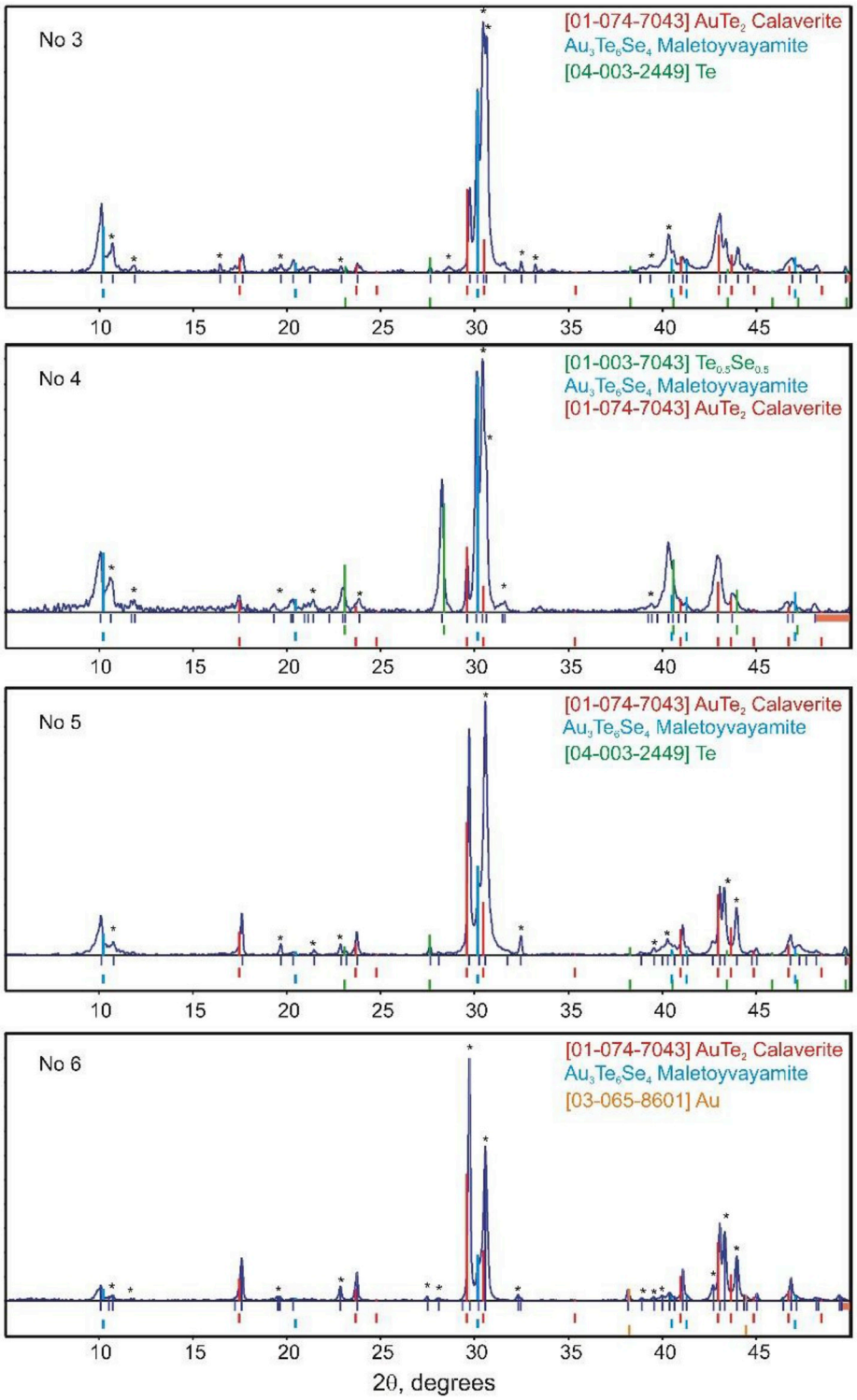

Fig. 3. Diffraction patterns of samples synthesized in experiments 3–6 (Tables 1 and 2). Peaks that were not clearly identified are marked by asterisks (see text for further explanation).

part, to $AuTe_2$–based phases (AuX_2). Although the position of the Au 4f lines essentially varied with the composition of Au chalcogenides [20, 40–45], experimental photoelectron spectra, including the spectra of the valence band (Figs. 6 and 7), X-ray absorption spectroscopy [46], and theoretical simulations [13,43] indicate that the oxidation state Au^{+} with fully occupied $5d^{10}$ band but not Au^{3+} (d^8) was common for all Au chalcogenides. Tellurium (Te $3d_{5/2}$ at 537.6 eV) bears a charge close to zero, while S and a share of Se atoms are charged negatively similar to sulfide and selenide anions. The structure of $Au_3Te_6Se_4$ phase [7], in which Au atoms are located in the center of cube faces, Te atoms sit at the edges, and Se occupies the vertices of the cube (Fig. 7), suggests an ionic type bonding between Au^{+} and Se^{2-} (S^{2-}) anions in Au_3X_{10}.

It is possible that the Au $4f_{7/2}$ peak at ~84.5 eV and Se $3d_{3/2}$ at 55 eV were due to the positive charge transfer from Au to ligand, which was previously proposed [13] and experimentally observed with XPS [43] for $AuTe_2$, when Se substitutes Te in Au_3X_{10} and AuX_2 compounds.

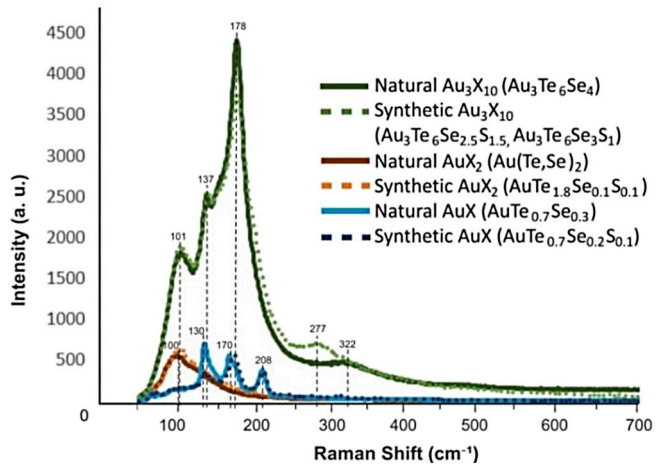

Fig. 4. Raman spectra of synthetic Au chalcogenides AuX, AuX_2 and Au_3X_{10} in comparison with natural analogs from the Gaching ore occurrence [35–37].

Moreover, the local charge at Se atoms and corresponding BEs seemed to depend on the total composition of the reaction mixtures and synthetic procedure, probably via the way in which Se and S substituted Te and each other. This suggests, for example, that Se atoms occupying positions of Te exhibited an enhanced BE of ~55 eV whereas neighboring Au atoms showed the Au $4f_{7/2}$ BE of ~84.5 eV. These effects should be further studied when employing pure materials.

4. Conclusions

This study reports the first results on Au compounds formed upon the interaction of Au^0 with a mixture of three chalcogens with the atomic ratios (Te + Se + S)/Au and Te/(S + Se) ranging within 1–4 and 1–2, respectively. Electron probe microanalysis and XRD showed Au chalcogenides with approximate composition $AuTe_{0.7}Se_{0.2}S_{0.1}$ (AuX) and yield of 10–15% or less, $AuTe_{1.8}(Se,S)_{0.2}$ (AuX_2) and $Au_3Te_6(Se,S)_4$ (Au_3X_{10}), where X indicates Σ(Te + Se + S). The phase Au_3X_{10} was characterized by variations in the content of S and Se in the range $Au_3Te_6Se_3S$–$Au_3Te_6Se_{2.5}S_{1.5}$, suggesting a series of solid solutions. For Au chalcogenides based on $AuTe_2$, isomorphic substitution of Te by S (up to 0.7 wt%) and Se (up to 2.9 wt%), corresponding to solid solutions $AuTe_2$–$AuTe_{1.8}Se_{0.2}$ and $AuTe_2$–$AuTe_{1.8}Se_{0.1}S_{0.1}$ was revealed. The Au_3X_{10} phases were close to S-bearing mineral maletoyvayamite, and the AuX substance seemed to be a synthetic analog of the mineral phase $Au_{0.99–1.00}Te_{0.70–0.71}Se_{0.25–0.27}S_{0.03–0.06}$ found in the Gaching area of the Maletoivayam ore field (Central Kamchatka volcanic belt). Raman spectra of synthetic Au chalcogenides AuX, AuX_2 and Au_3X_{10} were very similar to the natural phases. The XPS examination suggests, in particular, that Au was in the oxidation state of +1 and Te had the local charge approaching zero both in AuX_2 and Au_3X_{10}, while Se and S mainly occurred as selenide and sulfide anions. These results will be of interest for Au–chalcogenide chemistry, mineralogy and geochemistry, and potential applications in materials science.

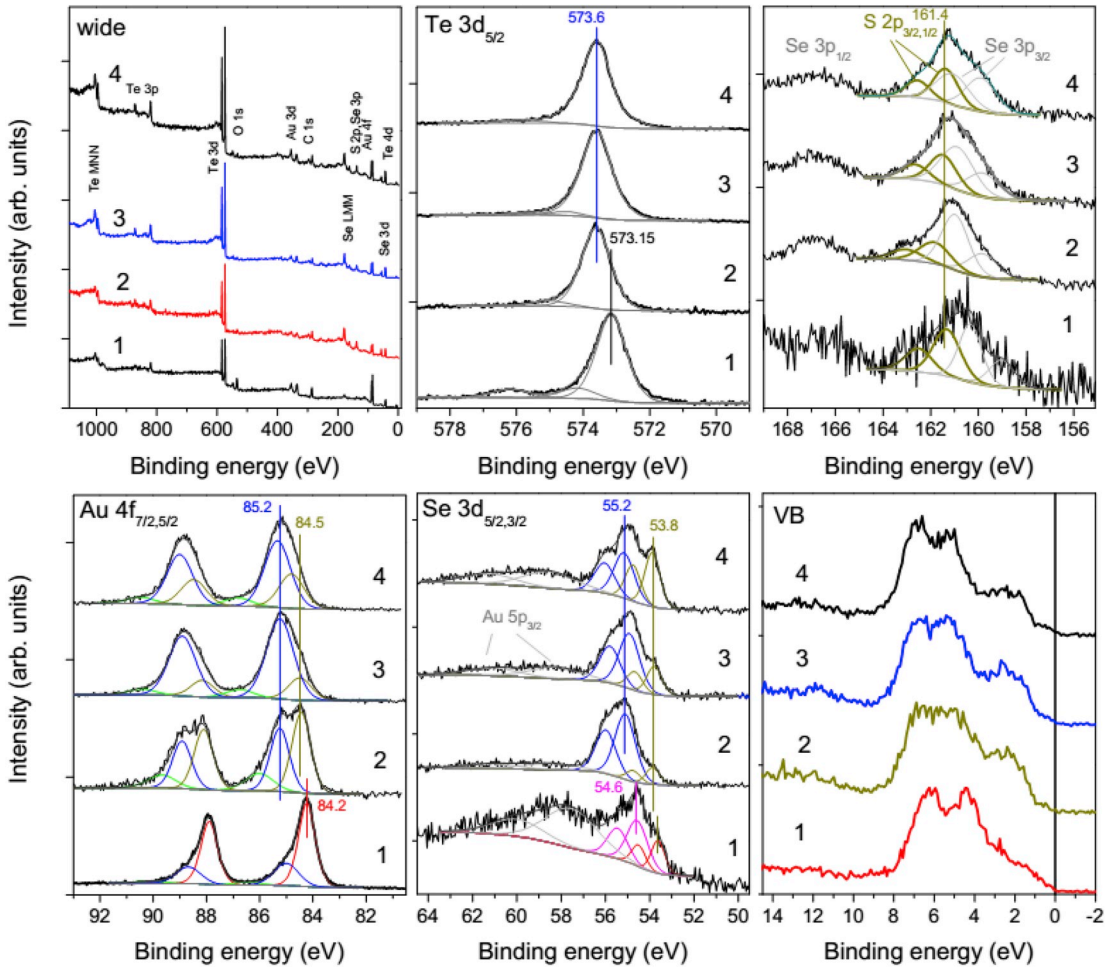

Fig. 5. X-ray photoelectron spectra (normalized in height) collected from samples 1–4 (Table 1) crushed before the measurement.

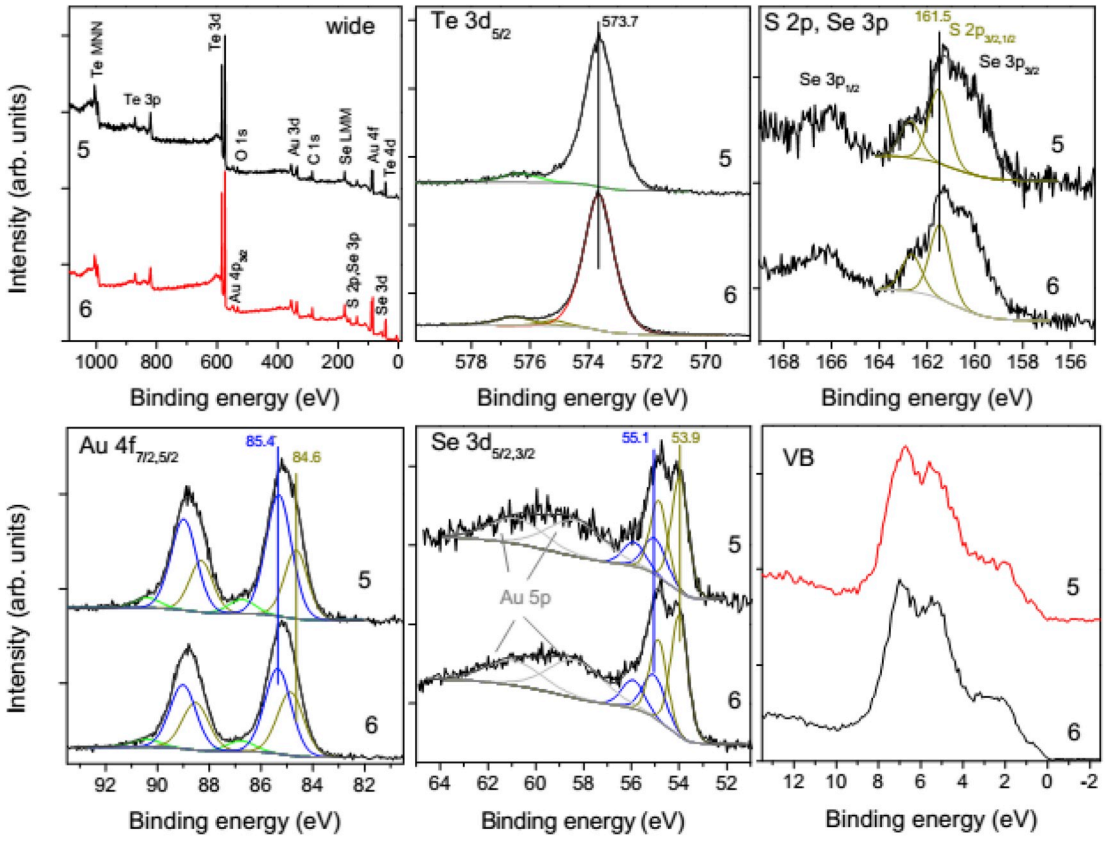

Fig. 6. X-ray photoelectron spectra collected from samples 5 and 6 (Table 2) crushed before the measurement.

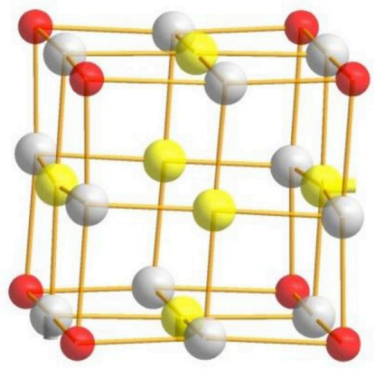

Fig. 7. A fragment of the crystal structure of maletoyvayamite [7]. Au atoms are yellow, Te atoms are gray and Se (S) anions are red.

Declaration of competing InterestCOI

The authors declare that they have no known competing financial interests or personal relationships that could have appeared to influence the work reported in this paper.

Credit author statement

G. Palyanova: Conceptualization, Methodology, Writing- Original draft preparation; Y. Mikhlin: Writing- Original draft preparation, Validation, Writing- Reviewing and Editing, Visualization; V. Zinina: Resources, Investigation, Visualization; K. Kokh: Investigation; Y. Seryotkin: Validation, Visualization; T. Zhuravkova: Formal analysis, Validation.

Acknowledgments

This work is supported by the Russian Foundation for Basic Research (Grant No. 19-05-00316a) and state assignments of IGM SB RAS and ICCT SB RAS financed by the Ministry of Science and Higher Education of the Russian Federation. The authors thank N.S. Karmanov (Institute of Geology and Mineralogy SB RAS) for the electron microprobe studies of polished sections. We are grateful to anonymous reviewers for their valuable comments and suggestions.

References

[1] G. Cranton, R. Heyding, The gold/selenium system and some gold seleno-tellurides, Can. J. Chem. 46 (1968) 2637–2640.
[2] F.E. Senftle, D.B. Wright, Synthesis of Au_2S and Au_2S_3 using H_2S, short-chain and ring-structured sulfur as sulfur sources, U.S. Geol. Surv. 86–179 (1986) 1081–1084.
[3] F. Bachechi, Synthesis and stability of montbrayite, Au_2Te_3, Am. Mineral. 57 (1972) 146–154.
[4] A.J. Criddle, C.J. Stanley, W.H. Paar, The optical properties of montbrayite, Au_2Te_3, from Robb Montbray, Quebec, compared with those of the other gold tellurides, Can. Mineral. 29 (1991) 223–229.
[5] H. Okamoto, T.B. Massalski, Bulletin of Alloy Phase Diagrams 5 (1984) 172–178.
[6] N.D. Wang, New synthetic ternary chalcogenides, Neues Jahrb. Mineral. Abh. 8 (2000) 348–356.
[7] M. Tuhý, A. Vymazalová, N.D. Tolstykh, J. Plášil, F. Laufek, M. Drábek, Precious Metals Chalcogenides, Experimental Study and Their Comparison to Natural Analogues, Abstract of 13 Pt Symposium, Polokwane, 2018, p. 199.
[8] L. Bindi, A. Arakcheeva, G. Chapius, The role of silver on the stabilization of the incommensurately modulated structure in calaverite, AuTe2, Am. Mineral. 94 (2009) 728–736.
[9] W. Jian, B. Lehmann, J. Mao, H. Ye, Z. Li, J. Zhang, H. Zhang, J. Feng, Y. Ye, Telluride and Bi-sulfosalt mineralogy of the Yangzhaiyu gold deposit, Xiaoqinling region, Central China, Can. Mineral. 52 (2015) 883–898.
[10] H.L. Luo, M.F. Merriam, D.C. Hamilton, Superconducting metastable compounds, Science 145 (1964) 581–583.
[11] J. Zhao, A. Pring, Mineral transformations in gold–(silver) tellurides in the presence of fluids: nature and experiment, Minerals 9 (2019) 167.
[12] Q.M.S. Rong, F.M. Liu, X.Y. Li, Y.F. Zhao, X.G. Jing, Study of small coinage metal telluride clusters Au_nTe_m (n, m = 1, 2), Chem. Pap. 61 (2007) 308–312.

[13] S.V. Streltsov, V.V. Roizenc, A.V. Ushakova, A.R. Oganov, D.I. Khomskiie, Old and new puzzles of gold tellurides: incommensurate crystal structure of calaverite $AuTe_2$ and predicted stability of AuTe, Proc. Natl. Acad. Sci. 115 (2018) 9945–9950.
[14] L.J. Cabri, Phase relations in the Au-Ag-Te system and their mineralogical significance, Econ. Geol. 60 (1965) 1569–1606.
[15] L. Fang, Y. Wang, M. Liu, M. Gong, A. Xu, Z. Deng, Dry sintering meets wet silver-ion "soldering": charge-transfer plasmon engineering of solution-assembled gold nanodimers from visible to near-infrared I and II regions, Angew. Chem. Int. Ed. 55 (2016) 14296–14300.
[16] A. Rabenau, H. Schulz, The crystal structures of α-AuSe and β-AuSe, J. Less Common. Met. 48 (1976) 89–101.
[17] E.A. Echmaeva, E.G. Osadchiy, Determination of the thermodynamic properties of a compound in the Ag-Au-Se and Ag-Au-Te systems by the EMF method, Geol. Ore Deposits 51 (2009) 276–288.
[18] D. Feng, P. Taskinen, Thermodynamic stability of AuSe at temperature from (400 to 700) K by a solid-state galvanic cell, J. Chem. Thermodyn. 71 (2014) 98–102.
[19] M.N. Short, Etch tests on calaverite, krennerite, and sylvanite, Am. Mineral. 22 (1937) 667–674.
[20] L.F.E. Machogo, P. Tetyana, R. Sithole, S.S. Gqoba, N. Phao, M. Airo, P. M. Shumbula, M.J. Moloto, N. Moloto, Unravelling the structural properties of mixed-valence - and -AuSe nanostructures using XRD, TEM and XPS, Appl. Surf. Sci. 456 (2018) 973–979.
[21] L. Bindi, W.H. Paar, G.O. Lepore, Montbrayite, $(Au,Ag,Sb,Pb,Bi)_{23}(Te,Sb,Pb,Bi)_{38}$, from the Robb-Montbray mine, Montbray, Québec: crystal structure and revision of the chemical formula, Can. Mineral. 56 (2018) 129–142.
[22] R.M. Thompson, The telluride minerals and their occurrence in Canada, Am. Mineral. 34 (1949) 342–382.
[23] N.L. Markham, Synthetic and natural phases in the system Au-Ag-Te, Econ. Geol. 55 (1960) 1148–1178.
[24] J.M. Shackleton, P.G. Spry, R. Bateman, Telluride mineralogy of the golden mile deposit Kalgoorlie, Western Australia, Can. Mineral. 41 (2003) 1503–1524.
[25] J. Wang, X. Lu, S. Bo, X. Su, Thermodynamic reassessment of the Au–Te system, J. Alloy. Comp. 407 (2006) 106–111.
[26] M.A. Peacock, R.M. Thompson, Montbrayite, a new gold telluride, Am. Mineral. 31 (1946) 515–526.
[27] J. Rucklidge, Frohbergite, montbrayite and a new Pb-Bitelluride, Can. Mineral., 1968, pp. 709–716.
[28] T.N. Chvileva, M.S. Bezsmertnaya, E.M. Spiridonov, A Reference-Guide to Ore Minerals in Reflected Light, Nedra, Moscow, 1988 (in Russian).
[29] F. Bachechi, Synthesis and stability of montbrayite, Au2Te3, Am. Mineral. 57 (1972) 146–154.
[30] I.K. Bonev, R. Petrunov, Cuprianmontbrayite, $(Au,Cu)_2Te_3$, associated with gold fieldite from the Chelopech Au-Cu deposit, Bulgaria, in: 32th Intern. Geol. Congr. 1, 2004.
[31] J.M. Shackleton, P.G. Spry, Antimony-rich montbrayite ($(Au,Sb)_2Te_3$) from the golden mile, Western Australia, and its compositional implications, Neues Jahrb. Mineral. Monatshefte (2003) 113–125, delete 2003 at the reference.
[32] J. Liu, M. Zheng, X. Liu, Au-Se paragenesis in Cambrian strata bound gold deposits, Western Qinling Mountains, China, Int. Geol. Rev. 42 (2000) 1037–1045.
[33] J. Liu, D. Zhaiang, H. Dai, Nanoscale characterization of Au_2Te grains from the Sandaowanzi deposit, Can. Mineral. 55 (2017) 181–194.
[34] O.Y. Plotinskaya, V.A. Kovalenker, R. Seltmann, C.J. Stanley, Te and Se mineralogy of the high-sulfidation Kochbulak and Kairagach epithermal gold telluride deposits (Kurama Ridge, Middle Tien Shan, Uzbekistan), Mineral. Petrol. 87 (2006) 187–207.
[35] N. Tolstykh, A. Vymazalová, M. Tuhý, M. Shapovalova, Conditions of formation of Au-Se-Te mineralization in the Gaching ore occurrence (Maletoyvayamore field), Kamchatka, Russia, Mineral. Mag. 82 (2018) 649–674.
[36] N.D. Tolstykh, G.A. Palyanova, O.V. Bobrova, E.G. Sidorov, Mustard gold of the gaching ore deposit (maletoyvayam ore field, Kamchatka, Russia), Minerals 9 (2019) 489, https://doi.org/10.3390/min9080489.
[37] G.A. Palyanova, N.D. Tolstykh, V.Yu Zinina, K.A. Kokh, YuV. Seryotkin, N. S. Bortnikov, Synthetic chalcogenides of gold in the Au-Te-Se-S system and their natural analogs, Dokl. Earth Sci. 487 (2019) 929–934, https://doi.org/10.1134/S1028334X19080099.
[38] N.D. Tolstykh, M. Tuhý, A. Vymazalová, J. Plášil, F. Laufek, A.V. Kasatkin, F. Nestola, Maletoyvayamite, IMA 2019-021. CNMNC newsletter No. 50, Eur. J. Mineral. 31 (2019) 850–851.
[39] The Powder Diffraction File PDF-4+, International Centre for Diffraction Data, Release, 2009.
[40] Y. Mikhlin, M. Likhatski, Y. Tomashevich, A. Romanchenko, S. Erenburg, S. Trubina, XAS and XPS examination of the Au-S nanostructures produced via the reduction of aqueous gold (III) by sulfide ions, J. Electron. Spectrosc. Relat. Phenom. 177 (2010) 24–29.
[41] Y. Mikhlin, A. Karacharov, M. Likhatski, T. Podlipskaya, I. Zizak, Direct observation of liquid pre-crystallization intermediates during the reduction of aqueous tetrachloroaurate by sulfide ions, Phys. Chem. Chem. Phys. 16 (2014) 4538–4543.
[42] S. Vorobyev, M. Likhatski, A. Romanchenko, N. Maksimov, S. Zharkov, A. Krylov, Y. Mikhlin, Colloidal and deposited products of the interaction of tetrachloroauric acid with hydrogen selenide and hydrogen sulfide in aqueous solutions, Minerals 8 (2018) 492.
[43] A. van Triest, W. Folkerts, C. Haas, Electronic structure and photoelectron spectra of calaverite, $AuTe_2$, J. Phys. Condens. Matter 2 (1990) 8733–8740.
[44] Y.L. Mikhlin, V.A. Nasluzov, A.S. Romanchenko, A.M. Shor, G.A. Pal'yanova, XPS and DFT studies of the electronic structures of AgAuS and Ag_3AuS_2, J. Alloy. Comp. 617 (2014) 314–321.
[45] Y.L. Mikhlin, G.A. Pal'yanova, Y.V. Tomashevich, E.A. Vishnyakova, S. A. Vorobyev, K.A. Kokh, XPS and Ag L_3-edge XANES characterization of silver- and silver-gold sulfoselenides, J. Phys. Chem. Solids 116 (2018) 292–298.
[46] A.R.H.F. Ettema, T.A. Stegink, C. Haas, The valence of Au in $AuTe_2$ and AuSe studied by X-ray absorption spectroscopy, Solid State Commun. 90 (1994) 211–213.